Properties of the H-T phase diagram of the 3-K phase in eutectic Sr_2RuO_4-Ru: Evidence for chiral superconductivity

Hirono Kaneyasu,[1,*] Yuya Enokida,[1] Takuji Nomura,[1,2] Yasumasa Hasegawa,[1] Toru Sakai,[1,2] and Manfred Sigrist[3,†]
[1]*Department of Material Science, University of Hyogo, Kamigori, Ako, Hyogo 678-1297, Japan*
[2]*National Institutes for Quantum and Radiological Science and Technology, SPring-8, Kouto, Sayo, Hyogo 679-5148, Japan*
[3]*Institute for Theoretical Physics, ETH Zurich, CH-8093 Zurich, Switzerland*

(Received 29 July 2019; published 3 December 2019)

We use the Ginzburg-Landau theory for a chiral p-wave superconductor to describe the filamentary superconducting phase nucleating at temperatures higher than the bulk transition temperature near the interfaces between Ru metal and Sr_2RuO_4 in eutectic Sr_2RuO_4-Ru. The peculiar phase diagram of magnetic field versus temperature shows very distinct properties for different directions of the magnetic field. A clear feature of the magnetic fields in the basal plane of Sr_2RuO_4, perpendicular to the chiral axis (c axis), is the occurrence of a second superconducting transition with a new order parameter visible as a zero-bias anomaly in tunneling spectroscopy. For the field along the c axis of Sr_2RuO_4, two transitions merge, indicating that the field drives the second-order parameter through the paramagnetic coupling to a chiral supercurrent. The resulting phenomenology shows that the assumption of a chiral superconducting order parameter in Sr_2RuO_4 yields an image reproducing the qualitative properties observed in the experiment. This discussion is qualitatively analogous to the corresponding chiral even- and odd-parity channels.

DOI: 10.1103/PhysRevB.100.214501

I. INTRODUCTION

Sr_2RuO_4 (SRO) is a quasi-two-dimensional metal with a layered perovskite crystal structure and is superconducting below a bulk transition temperature $T_{c,\mathrm{SRO}} = 1.5$ K [1]. This property has been experimentally shown for unconventional Cooper pairing with a two-component order parameter [2–5]. Broken time-reversal symmetry concluded from muon spin rotation (μSR) measurements [6,7] and the observation of a polar Kerr effect [8] point toward a superconducting phase with twofold degeneracy. This is corroborated, for example, by the behavior of the ultrasound velocity for transverse modes at the superconducting transition [9–13] and the finding of unusual saddle points in the flux distribution of the mixed state for fields along the c axis [14]. Following the standard classification scheme of Cooper pairing symmetries in a tetragonal crystal, there are two unitary states, which are both chiral: the even-parity "d-wave" state represented by the scalar gap function of the basic form $\psi(\boldsymbol{k}) = \Delta_0 k_z(k_x \pm ik_y)$ and the odd-parity "p-wave" state, which is given in the vector form as $\boldsymbol{d}(\boldsymbol{k}) = \Delta_0\hat{\boldsymbol{z}}(k_x \pm ik_y)$ [15,16]. The former is a spin-singlet state based on interlayer pairing, and the latter corresponds to in-plane equal-spin pairing (spin triplet with $S_z = 0$), where the paired electrons lie in the same plane. While the NMR-Knight-shift data appeared to clearly support the in-plane equal-spin pairing state [17,18], recent experiments have shown that the susceptibility is reduced in the superconducting phase for in-plane fields because it is more compatible with the even-parity spin-singlet phase [19,20]. The in-plane upper critical field displays features analogous to paramagnetic limiting, which is in agreement with the above-mentioned result [4,21–23]. However, Josephson tunneling experiments such as the test of selection rules and superconducting quantum interface device (SQUID) experiments connecting an s-wave superconductor with junctions on opposite in-plane faces of SRO support odd-parity pairing symmetry [24–26]. Moreover, the observation of half-flux quanta in micrometer-sized loops of SRO [27–29] is readily interpreted in terms of an odd-parity state through the additional degree of freedom of the $\boldsymbol{d}$-vector orientation [30,31].

In this context, the discussion of the nodal structure of the gap is important, in particular, because the even-parity state has a symmetry-imposed horizontal line node for $k_z = 0$, while no nodes are required for the odd-parity state for cylindrical Fermi surfaces as realized in SRO [3]. Thermodynamic experiments provide clear evidence for nodal structures or at least strong gap anisotropy [32–34]. However, these results lead to conflicting interpretations for the location and orientation of gap nodes, either vertical [32] or horizontal [34]. Moreover, the quantitative discussion of thermodynamic quantities is complicated because SRO has three Fermi surfaces [3].

Both time-reversal symmetry-breaking states, in principle, generate spontaneous in-plane edge currents and corresponding local magnetic flux near surfaces [35,36]. Regardless of the highly sophisticated investigations, such magnetic flux has not been detected thus far [37–40]. This could be attributed to the fact that the magnitude of the charge currents of these

*hirono@sci.u-hyogo.ac.jp
†sigrist@itp.phys.ethz.ch

chiral superconducting states is not universal and is affected by various factors, in particular, the surface properties [41–43].

In the following we analyze a set of experiments under the assumption that the pairing state has the chiral symmetry represented by $k_x \pm ik_y$, which incorporates the essential feature of an intrinsic Cooper pair angular moment $L_z = \pm 1$ along the crystalline c axis. This aspect is common to both the chiral p-wave and d-wave states introduced above. Both states are represented by two complex order parameter components: $(\eta_x k_x + \eta_y k_y)$ with $\boldsymbol{\eta} = (\eta_x, \eta_y) = \Delta_0(1, \pm i)$, where Δ_0 denotes the gap magnitude. By symmetry both chiral states are described by the Ginzburg-Landau (GL) free energy of the very same structure. While the distinct gap anisotropies will lead to quantitative differences, the qualitative behavior would be the same in both cases.

The degeneracy of the two order parameter components can be lifted by symmetry reduction, which can be achieved by uniaxial pressure [44]. This should lead to two consecutive superconducting transitions. The second transition would be the spontaneous time-reversal symmetry breaking. Thus far, the uniaxial compressive stress experiments do not seem to be in agreement with this symmetry argument [44–46]. However, very recent μSR measurements signal a time-reversal symmetry-breaking second transition below the onset of superconductivity in uniaxially strained samples which would support the picture of two degenerate order parameter components [47].

An alternative method for removing the degeneracy of the two components is to confine the sample geometry of the superconducting condensate along one of the two in-plane directions. Such conditions are likely realized in a rather unexpected way in eutectic SRO-Ru samples, where micrometer-sized Ru metal inclusions are immersed in SRO. In such samples, an inhomogeneous superconducting phase appears at $T_c' \approx 3$ K above the superconducting bulk transition [48]. There is good experimental evidence that this phase, called the 3-kelvin phase (3-K phase), has a filamentary nature. It nucleates at the interface between SRO and Ru metal, mainly within SRO, due to locally enhanced pairing and decays towards the bulk [49–51]. In this manner, the nucleating superconducting condensate is confined to a length scale comparable to the coherence length and exists in an environment of reduced symmetry, i.e., the direction along and perpendicular to the interface. For the enhancement, various mechanisms had been proposed, such as the effect of local strains near the interface [51], increased ferromagnetic spin fluctuations [52], the influence of edge dislocations [53], and Lifshitz transition by stress [45] near the Ru inclusion, to mention a few.

The unconventional nature of the 3-K phase was corroborated by the observation of a zero-bias anomaly in the differential quasiparticle tunneling conductance [54,55]. The setup of this measurement by Kawamura *et al.* relies on tunneling through a Ru-SRO interface, where a single Ru inclusion at the surface of the sample is contacted [55]. The zero-bias anomaly suggests the presence of subgap Andreev bound quasiparticle states at the tunneling interface, a characteristic of unconventional pairing states. They appear at a transition temperature of $T^* \approx 2.3$ K, well below the nucleation of the 3-K phase and above the onset of bulk superconductivity.

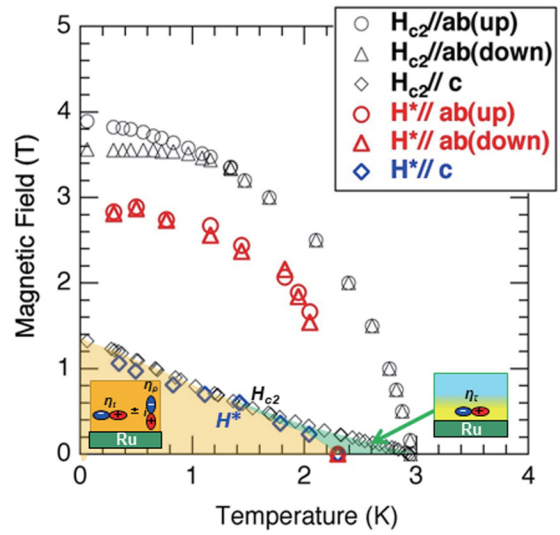

FIG. 1. H-T phase diagram for H_{c2} and H^* for the onset of the 3-K phase and the appearance of the zero-bias anomaly in quasiparticle tunneling, respectively [59]. For fields $\boldsymbol{H} \parallel \boldsymbol{c}$ the critical fields are marked by diamonds, and for $\boldsymbol{H} \parallel \boldsymbol{ab}$ (in plane) circles and triangles are used. In the zero magnetic field, the onset temperature is approximately 3 K, and the second transition occurs at approximately 2.3 K. For in-plane fields, the "up" (circles) and "down" (triangles) ramping fields are displayed to show that H_{c2} exhibits hysteretic behavior at very low temperatures, a feature not addressed in our theory. The pictorial insets show the difference of the filamentary state for the case of the c-axis field. This figure has been adapted from Ref. [59].

Along with the observation of anomalous properties of the critical current for $T < T^*$ [56], this provides good evidence for a second phase transition that breaks time-reversal symmetry and is in good agreement with the expectations for a chiral superconductor [57,58].

In the present study, we show that the properties of the second transition above $T_{c,\mathrm{SRO}}$ allow for important conclusions on the symmetry of the order parameter if we analyze the behavior in an external magnetic field. Owing to the filamentary nature of the nucleating superconductivity, the upper critical field of the 3-K phase is strongly enhanced compared with the bulk $H_{c2,b}$, exceeding in the limit $T \to 0$ K the value $H_{c2} = 1$ T for fields along the c axis and reaching 4 T for in-plane fields (see Fig. 1) compared to the bulk $H_{c2,b} = 0.075$ and 1.5 T, respectively. The confinement of the superconducting state to the region close to the Ru-SRO interface is additionally responsible for the sublinear temperature dependence of H_{c2} close to T_c', i.e., $H_{c2} \propto |T - T_c'|^\alpha$, with $0.5 < \alpha < 1$ and the upturn at low temperatures for fields along the c axis (Fig. 1), as has been discussed in detail in Ref. [60] based on data of Ref. [49]. Based on their systematic analysis of tunneling spectroscopy data, Kawamura *et al.* obtained the H-T phase diagram identifying the second transition (critical field H^*) through the onset of the zero-bias anomaly (Fig. 1) [55,59]. The difference between the two field directions is interesting. For the in-plane fields, H^* lies well below the corresponding H_{c2} of the nucleation of the 3-K phase for all temperatures $T < T^*$. In contrast, for fields parallel to the c axis, H^* rapidly merges with the corresponding H_{c2} and, for

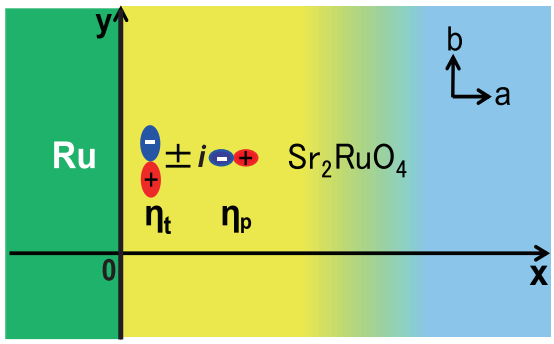

FIG. 2. The 3-K phase model with a planar Ru metal interface perpendicular to the RuO_2 plane. The interface superconducting state is located near the Ru-SRO interface. In the representation of the d vector $\boldsymbol{d} = z(\eta_t k_t + i\eta_p k_p)$, η_p and η_t correspond to components perpendicular and tangential to the interface, respectively. Note that $\eta_t k_t + i\eta_p k_p$ is assumed to cover both the chiral even- and odd-parity channels.

$T < 1.8$ K, is essentially identical to H_{c2}. These will be the main features we aim at explaining within our model. Note that in Fig. 1 of Ref. [59] the H-T phase diagram was also examined for hysteretic behavior of the transition for in-plane fields. Therefore, the data for increasing (up) and decreasing (down) fields are displayed, unlike for the c-axis field. This led to the discovery of a hysteresis for the nucleation of the 3-K phase at rather low temperature, a feature which, however, lies outside the scope of our discussion.

For our discussion of the H-T phase diagram, we decompose the superconducting order parameter of the 3-K phase into two components (here written for the p-wave state): $\boldsymbol{d}(\boldsymbol{k}) = \hat{z}(\eta_t k_t + \eta_p k_p)$, which correspond to the tangential momentum direction k_t and k_p, perpendicular to the interface, with the corresponding order parameters η_t and η_p (see Fig. 2). At the onset of the 3-K phase, only the component η_t nucleates at the interface owing to a locally enhanced transition temperature (the origin of this enhancement is still unknown) and decays toward the bulk of SRO. This phase does not break the time-reversal symmetry. At a lower temperature, $T^* \approx 2.3$ K, the second component η_p appears with a relative phase of $\pm\pi/2$, leading to the breaking of time-reversal symmetry. The interface affects the two components differently owing to their distinct symmetries. The tangential component η_t is under the reflection of a mirror plane parallel to the interface, and its Cooper pair wave function has constructive interference. In contrast, the perpendicular component η_p is odd and suffers from destructive interference (Cooper pair breaking), accompanied by subgap Andreev bound states. These result in zero-bias anomalies in tunneling spectroscopy [55,61]. In this manner, H^* traces the onset of the perpendicular order parameter component, corresponding to the second transition. We consider the behavior of H^* for a phenomenological GL approach and show that it agrees well within the results of a chiral superconducting phase in SRO. In this study, we show the chiral stability in the 3-K phase in the magnetic field by the GL theory, which explains the field dependence of H^* in Fig. 1. We also clarify that this field-induced chiral stability in the interface state causes paramagnetic supercurrents and a change in chirality at a certain distance.

II. GINZBURG-LANDAU THEORY FOR THE 3-K PHASE

We introduce our GL theory that models the situation near the Ru-SRO interface, where we restrict the study to the SRO side (see Fig. 2). For the order parameter, we use the two components (η_t, η_p) from $\boldsymbol{d}(\boldsymbol{k}) = \hat{z}(\eta_t k_t + \eta_p k_p)$. We assume that the interface lies on the plane with normal vector $\boldsymbol{n} = (1, 0, 0)$ (b-c plane) and is located at $x = 0$. Although $k_p = k_x$ and $k_t = k_y$, we will keep the indices (p, t) following the discussion above. Assuming homogeneity along the y and z directions, the GL free-energy functional (per unit area of the interface) is given as

$$
\begin{aligned}
F = \int_0^\infty dx \Bigg[& a(T,x)(|\eta_p|^2 + |\eta_t|^2) + \frac{b}{4}\Big\{\frac{3}{2}(|\eta_p|^2 + |\eta_t|^2)^2 \\
& - |\eta_p|^2|\eta_t|^2 + \frac{1}{2}(\eta_p^{*2}\eta_t^2 + \eta_p^2\eta_t^{*2})\Big\} \\
& + K_1(|D_x\eta_p|^2 + |D_y\eta_t|^2) + K_2(|D_y\eta_p|^2 + |D_x\eta_t|^2) \\
& + \big\{K_3(D_x\eta_p)^*(D_y\eta_t) + K_4(D_x\eta_t)^*(D_y\eta_p) + \text{c.c.}\big\} \\
& + K_5(|D_z\eta_p|^2 + |D_z\eta_t|^2) + \frac{1}{8\pi}|\nabla \times \boldsymbol{A} - \boldsymbol{H}|^2\Bigg], \qquad (1)
\end{aligned}
$$

where the gradient $\boldsymbol{D}$ is defined as $\boldsymbol{D} = \nabla - i\gamma\boldsymbol{A}$, with $\gamma = 2e/\hbar c$, and the vector potential $\boldsymbol{A}$ is related to the total magnetic field $\boldsymbol{B}$, $\boldsymbol{B} = \nabla \times \boldsymbol{A}$. The second-order coefficient has a position-dependent critical temperature $a(T,x) = a'\{[T - T_c(x)]/T_{c,\text{SRO}}\}$, with $a' > 0$ and $T_c(x) = T_{c,\text{SRO}} + T_0/\cosh[x/w]$, which describes a layer of enhanced critical temperature relative to $T_{c,\text{SRO}} = 1.5$ K [51,57,62]. The layer width is denoted by w, which is several tens of a nanometer [60]. The other coefficients, b and K_i, are real and positive. Assuming a cylindrical Fermi surface, we find the relations $a' = 15b/4$ and $K_1 = 3K_{2,3,4} = 150K_5$, where $K_1/a' = \xi_0^2$ and ξ_0 defines the zero-temperature coherence length ($\xi_0 \sim w$). Note that the very small value for K_5 is because of the quasi-two-dimensional structure of SRO and leads to the highly anisotropic bulk upper critical field. It can be clearly seen that the homogeneous phase in bulk SRO for $T < T_{c,\text{SRO}}$ is given by the order parameter $(\eta_t, \eta_p) = \eta_0(1, \pm i)$; that is, it is chiral.

The boundary conditions are derived after adding a simple interface term to F, $F_{\text{int}} = g_p|\eta_p(x=0)|^2$, which describes the suppression of η_p through pair breaking, while the η_t component remains unaffected. Thus, the variational boundary conditions for the two order parameter components are given by

$$K_1\partial_x\eta_p|_{x=0} = g_p\eta_p(0), \qquad (2)$$

$$K_2\partial_x\eta_t|_{x=0} = 0. \qquad (3)$$

Note that $g_p = 1/l_p$, where l_p is the so-called extrapolation length. The scanning transmission electron microscopy (STEM) measurements have shown that the Ru-SRO interfaces are atomically sharp and regular, suggesting specular scattering on short length scales [63].

We now consider the situation where an external magnetic field is applied. The highest critical temperatures are obtained when the applied fields lie parallel to the interface. Thus, we consider two cases in the Landau gauge: in-plane fields $\boldsymbol{H} = (0, H, 0) \parallel \hat{\boldsymbol{y}}$ with a vector potential $\boldsymbol{A} = (0, 0, -Hx)$

and c-axis fields $\boldsymbol{H} = (0, 0, H) \parallel \hat{\boldsymbol{z}}$ with $\boldsymbol{A} = (0, Hx, 0)$. It is illustrative to consider the gradient terms for the two field directions. First, we consider the in-plane field, $\boldsymbol{H} \parallel \hat{\boldsymbol{y}}$, where the free-energy density of the gradient terms is given by $f_K = f_1 + f_2$, with

$$f_1 = K_1|\partial_x \eta_p|^2 + K_2|\partial_x \eta_t|^2, \tag{4}$$

$$f_2 = (\gamma A_z)^2 K_5(|\eta_p|^2 + |\eta_t|^2), \tag{5}$$

which yields a suppression for both components by the magnetic field. For $\boldsymbol{H} \parallel \hat{\boldsymbol{z}}$, the free-energy density has three terms, $f_K = f_1 + f_3 + f_4$:

$$f_3 = (\gamma A_y)^2\{K_1|\eta_p|^2 + K_2|\eta_t|^2\}, \tag{6}$$

$$f_4 = -i\gamma A_y\{K_3(\partial_x \eta_p)^* \eta_t - K_4 \eta_p^*(\partial_x \eta_t) - \text{c.c.}\}. \tag{7}$$

While f_3, analogous to f_2, yields a suppression for both components, f_4 combines the two order parameter components such that both η_p and η_t are present. In addition, the boundary conditions for a nonvanishing field are augmented for $\boldsymbol{H} \parallel \hat{z}$,

$$K_1 \partial_x \eta_p|_{x=0} = g_p \eta_p(0) - i\gamma A_y(0) K_3 \eta_t(0), \tag{8}$$

$$K_2 \partial_x \eta_t|_{x=0} = i\gamma A_y(0) K_4 \eta_p(0), \tag{9}$$

which also favors the appearance of the two order parameter components together. The boundary conditions as well as the f_4 term favor the chiral combinations such that η_p has the relative phase $\pm\pi/2$ with η_t, where the sign is determined by the field orientation.

We also consider the expression for the supercurrents parallel to the interface. These are obtained by varying the free-energy functional F with respect to $\boldsymbol{A}$. We obtain

$$\begin{aligned} j_y(x) = 8\pi[&-\gamma^2 A_y(K_1|\eta_p|^2 + K_2|\eta_t|^2) \\ &- i\gamma\{K_3 \eta_t^*(\partial_x \eta_p) - K_4(\partial \eta_t)\eta_p^* - \text{c.c.}\}] \end{aligned} \tag{10}$$

for the y component. The first term describes the screening current density j_y^s for magnetic fields $\boldsymbol{H} \parallel \hat{\boldsymbol{z}}$, and the second corresponds to a current density j_y^c when the order parameter forms a chiral superconducting state. For the z component, we find

$$j_z(x) = -8\pi\gamma^2 A_z K_5(|\eta_p|^2 + |\eta_t|^2), \tag{11}$$

which is a screening current for $\boldsymbol{H} \parallel \hat{\boldsymbol{y}}$.

The stable order parameter configuration in a magnetic field can be obtained by solving the variational GL equation of F, including the boundary conditions. We address this problem numerically using the Newton-Euler method that allows us to obtain the exact solution of a nonlinear differential equation. To adapt our values to practical scenarios, we use the following parameters: $T_0 = 2$ K, $w = 0.5$ for the unit length ξ_0. We choose $a' = 1$ and $l_p = 4.6$. In this manner, the onset of the 3-K phase occurs at $T_c' \approx 3$ K, and the second transition where η_p appears is at $T^* \approx 2.3$ K. Moreover, γ is fixed through the relation $H_{c2,b} = (\xi_0^2 \gamma)^{-1} = 0.075\ \text{T} = H_0$, which we use as the unit for magnetic fields.

III. NUMERICAL RESULTS AND ANALYSIS

A. Phase diagram

Now, we consider the results obtained by computationally solving the GL equations focusing on the H-T phase diagram of the 3-K phase. For this, we scan the H-T plane by fixing T and varying H (see Fig. 3 and Fig. 4). The results for the field direction, $\boldsymbol{H} \parallel \hat{\boldsymbol{z}}$ are displayed in Fig. 3, showing the behavior of the two order parameter components. For these graphs, we choose the maximal values of the x-dependent $\eta_{t,p}^m$. A more detailed discussion of the structure of the order parameter near the interface is given below and displayed in Figs. 6 and 8. For $H_z = 0$, we find that η_t^m appears at $T_c' = 3$ K, while η_p^m remains zero until the temperature of the second transition, $T^* \approx 2.3$ K, is attained. This is in good agreement with the discussion above that the onset of the 3-K phase leads to a nonchiral state consisting only of the order parameter component that is tangential to the interface. However, for nonvanishing H_z, both order parameter components become finite below the upper critical field $H_{c2}(T)$. The perpendicular component η_p^m is clearly field induced, as the contour lines in the graph exhibit a bulge for higher temperatures. This indicates that for $H \neq 0$ also $|\eta_p^m| \neq 0$ for $T > T^*$. The magnitude of η_p^m remains in the range $T^* < T < T_c'$, which is small. The important additional features we recognize in Fig. 3 are that the two order parameter components share the same upper critical field $H_{c2}(T) = H^*(T)$. For $T \lesssim T^*$, both η_t^m and η_p^m have comparable magnitudes. The qualitative difference between $T > T^*$ and $T < T^*$ can be seen in Fig. 5, where the field dependence of both components is shown for $T = 2.1$ and 2.5 K. For the latter, the role of the magnetic field in driving the perpendicular component becomes apparent. The overall behavior is consistent with the experimental finding from the detection of the zero-bias anomaly.

This is in contrast to the same type of plots for the in-plane fields, $\boldsymbol{H} \parallel \hat{\boldsymbol{y}}$ (see Fig. 4). First, the upper critical field $H_{c2} \parallel \hat{\boldsymbol{y}}$ for the onset of the 3-K phase is considerably higher, in our calculation approximately by a factor of 10 and in experiment between a factor of 3 and 4. At H_{c2}, the tangential component η_t^m vanishes. At $H_y = 0$, the behavior is the same as in the analog case of $H_z = 0$ with the second transition at T^* where, the perpendicular component of the order parameter appears. The magnetic field suppresses η_p^m with a critical field $H^*(T)$, which is considerably smaller than $H_{c2}(T)$ for all temperatures. This is a qualitative difference; the above case is in good agreement with the experimental results displayed in Fig. 1. Clearly, η_p^m is constant at zero above T^* and also for $H_y \neq 0$, such that the phase boundary $H^*(T)$ represents a second symmetry-breaking transition, leading to a chiral order parameter.

B. Properties for c-axis fields

As we mentioned earlier, the coupling of the magnetic field to the order parameter is unusual for $\boldsymbol{H} \parallel \hat{\boldsymbol{z}}$. The magnetic field is considered through the gradient terms f_K, while the terms f_2 and f_3 in Eqs. (5) and (6) yield the usual suppression of the superconductivity by a magnetic field by increasing the energy (origin for the screening currents). The term f_4 in Eq. (7) involves η_t and η_p such that it is possible to increase energy by

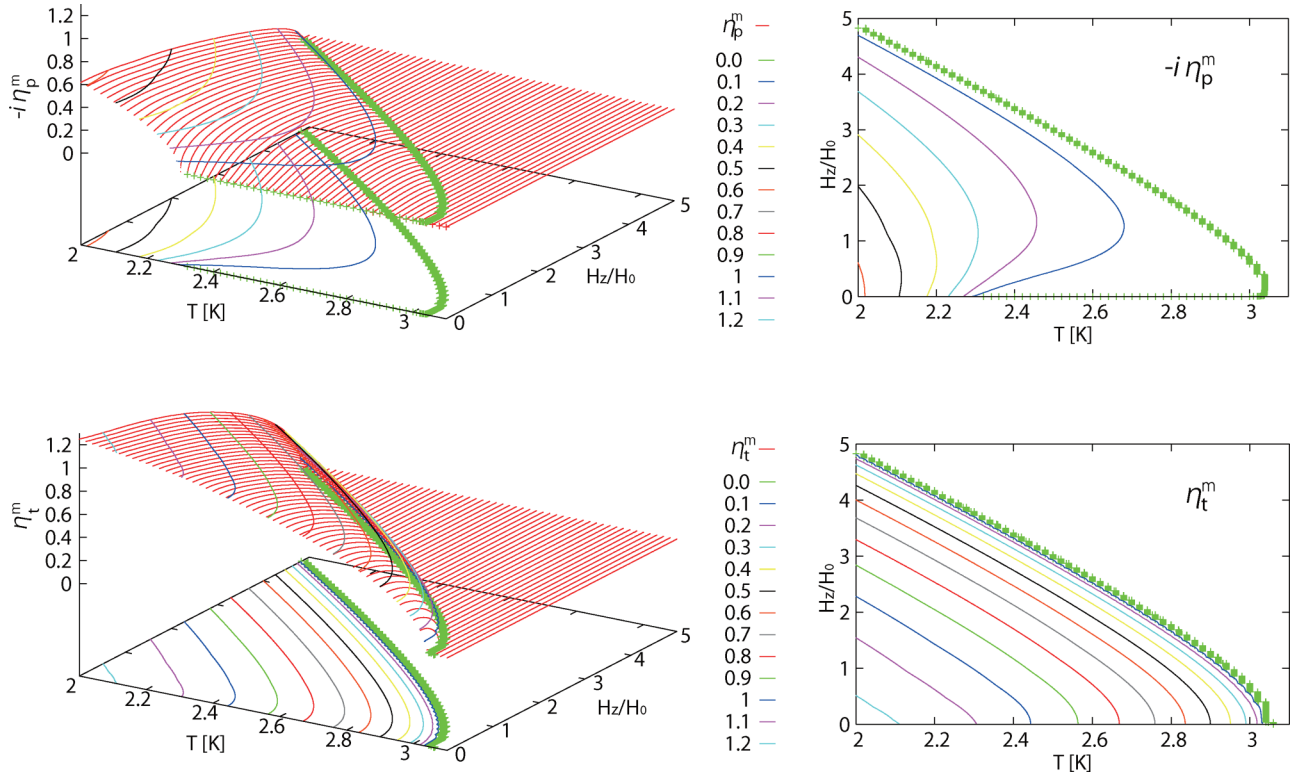

FIG. 3. Temperature and field dependence of the order parameter components η_p and maximum η_t for $\boldsymbol{H} \parallel z$: We display the maximal value of the order parameters as a function of the position. The thick green line indicates H_{c2}. The contour lines show that η_p is induced by the magnetic field, as it develops a bulge at temperatures higher than $T^* \approx 2.3$ K. The η_t component is suppressed by the magnetic field. The magnetic field is given in units of $H_0 = 0.075$ T such that the largest field is $H_z = 5H_0 = 0.375$ T, comparing well with the experimental value at $T = 2$ K in Fig. 1.

coupling to the magnetic field. This require the spatial variation of the order parameter components and that their relative phase is different from 0 and π, optimally $\pm\pi/2$, whereby the sign is determined by the field orientation. The term f_4 describes the coupling of the magnetic field to the angular momentum of the Cooper pairs. It can also be written using the spontaneous chiral current j_y^c included in the second term of $j_y(x)$ in Eq. (10) through $f_4 = -A_y j_y^c$, which corresponds to paramagnetic coupling. Note that the boundary conditions in Eqs. (8) and (9) originate from the same mechanism. Thus, the fact that the magnetic field induces η_p for $T > T^*$ can also be considered indirect evidence of the existence of chiral currents in relation to interface superconductivity, beyond simple screening currents.

Finally, we consider the spatial dependence of the order parameter components for temperatures above and below T^*. In Fig. 6, we show the situation for $T = 2.5$ K with and without a magnetic field. For $H_z = 0$, only the tangential component is nonvanishing and falls on a length scale of a few ξ_0 to zero away from the interface. For $H_z \neq 0$, the perpendicular component η_p appears, induced by the field. For the same temperature, Fig. 7 shows the current density composed of the screening current j_y^s and j_y^c. The screening current comprises two counterpropagating currents that yield a magnetization opposite the uniform external field. The chiral currents show the opposite feature contributing to the magnetization parallel to the external field. It is clear that this corresponds to the paramagnetic coupling responsible for the driving of η_p, as mentioned above. Lowering the temperature to $T = 2.1$ K leads to the regime where both order parameter components are nonvanishing, even in the zero field. In a finite magnetic field, a slight modification is observed, as shown in Fig. 8.

Note that, for finite magnetic fields, η_t changes sign at approximately $x \sim 1$ (the coherence length), which corresponds to a reversal of chirality. While this constitutes, in principle, a domain wall (see Fig. 9) and may be counterintuitive in this situation where an external magnetic field should actually favor only one of the two domains, analyzing the gradient term f_4 in Eq. (7) shows that in this way the energy gain through the paramagnetic coupling to the magnetic field can be maximized [64]. In this context, the difference in the length scales $\xi_{p,t}$ of decay for η_p and η_t, where ξ_p is longer than ξ_t, is important. However, it is unclear whether this peculiar feature would lead to any observable effect.

IV. CONCLUSIONS

Our discussion showed that the model of a filamentary superconducting phase nucleating at the interface of Ru and SRO, based on the assumption of a chiral pairing state for SRO, can account for the basic properties of the H-T phase diagram of the 3-K phase (see Fig. 1) [55,59]. In particular, this model provides an understanding of the difference of the two magnetic field directions, in plane and out of plane. However, the first important aspect of this model is the presence of two superconducting transitions, which is very visible in

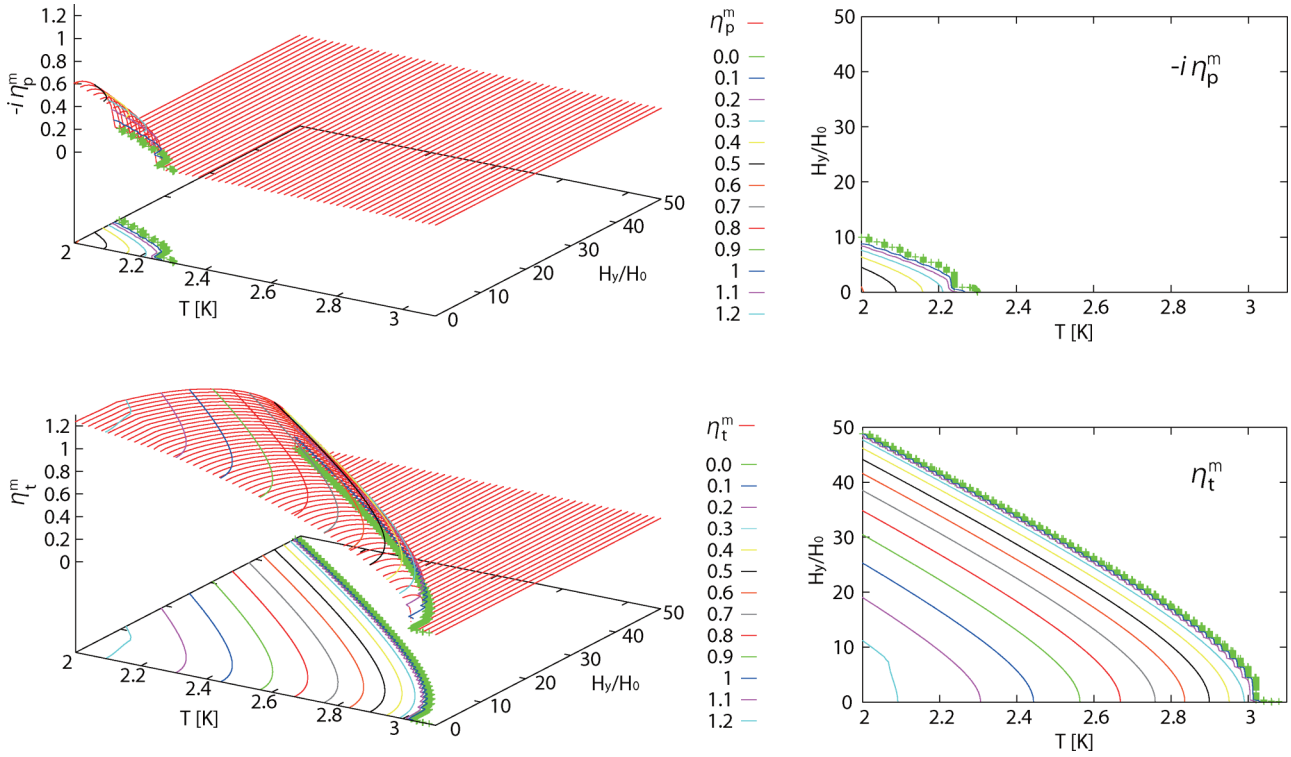

FIG. 4. Temperature and field dependence of the order parameter components η_p and maximum η_t for $\boldsymbol{H} \parallel \boldsymbol{y}$: We display the maximal value of the order parameters as a function of position. The thick green line indicates H_{c2}. The contour lines show that both components are suppressed by the magnetic field, and η_p appears only below H^*, being strictly smaller than H_{c2}. The largest field is $H_y = 50H_0 = 3.75$ T, comparing well with the experimental value at $T = 2$ K in Fig. 1.

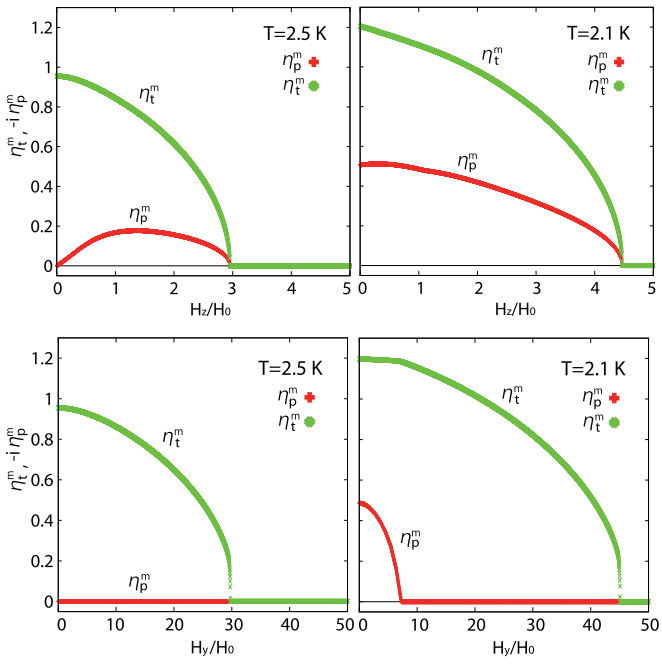

FIG. 5. Field dependence of the order parameter for temperature $T = 2.5$ K $> T^*$ and $T = 2.1$ K $< T^*$: The top two panels show the behavior of $\boldsymbol{H} \parallel \boldsymbol{z}$, and the bottom panels show $\boldsymbol{H} \parallel \boldsymbol{y}$. For the former case, it is clear that η_p is field driven for $T > T^*$. In the latter case, η_p remains strictly zero for T^*.

the phase diagram for the in-plane field. In this case, we see an upper critical field H_{c2} for the onset of the filamentary 3-K phase (detected through the drop in electrical resistance) and a second critical field H^* suggesting the appearance of a second-order parameter signaled by the rise of a zero-bias anomaly in the tunneling spectroscopy. An even more

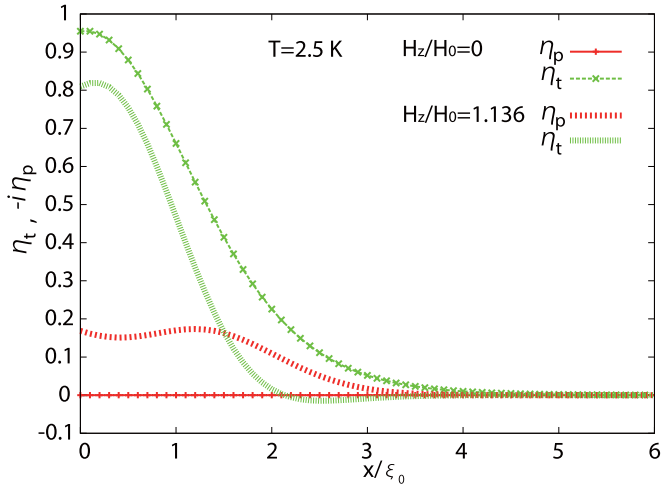

FIG. 6. Spatial dependence of the order parameter components with and without magnetic field $\boldsymbol{H} \parallel \boldsymbol{z}$ for $T = 2.5$ K $> T^*$. x is given in units of ξ_0. The magnetic field used in the graph $H_z = 1.136H_0 = 0.085$ T.

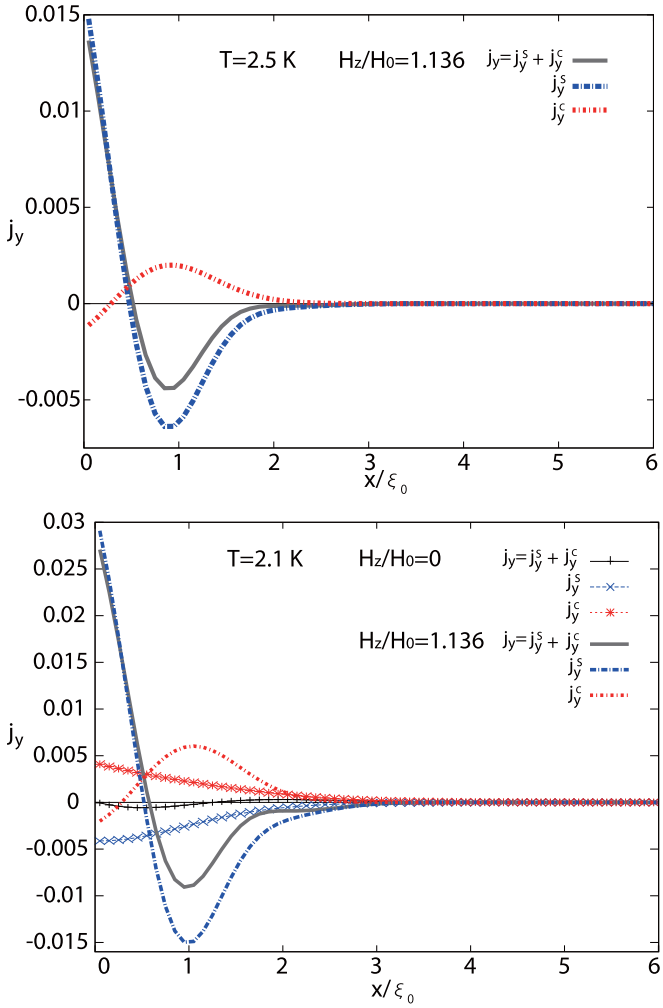

FIG. 7. Spatial dependence of the current density j_y for $\boldsymbol{H} \parallel \boldsymbol{z}$ at $T = 2.5$ K (top panel) and 2.1 K (bottom panel). We distinguish between screening current density j_y^s and chiral current density j_y^c, where the total current density is the sum of the two. The magnetic field used in the graph is $H_z = 1.136H_0 = 0.085$ T.

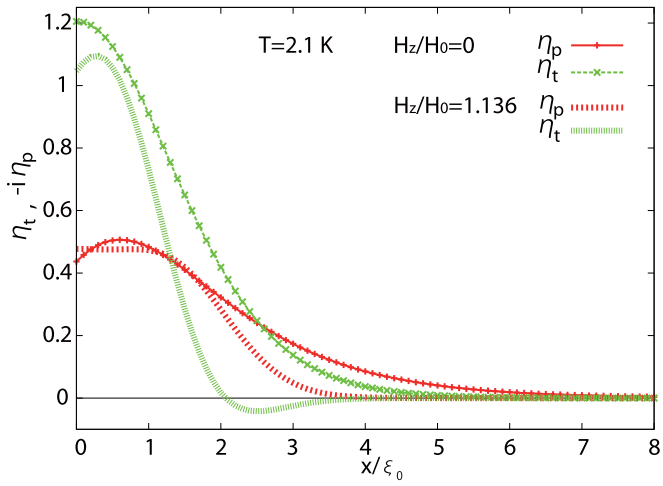

FIG. 8. Spatial dependence of the order parameter components with and without magnetic field $\boldsymbol{H} \parallel \boldsymbol{z}$ for $T = 2.5$ K $> T^*$. In a finite magnetic field, the η_t component changes sign away from the interface. The magnetic field used in the graph is $H_z = 1.136H_0 = 0.085$ T.

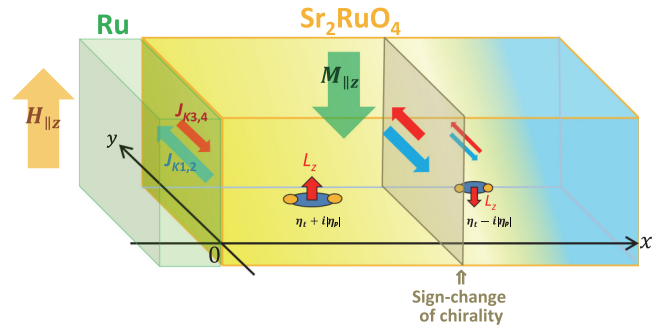

FIG. 9. Inversion of chirality is induced by an energy gain to optimize the coupling of the external field to the paramagnetic current.

intriguing and crucial property is observed in the phase diagram for the c-axis field, where H^* merges with H_{c2}. This indicates the removal of the second transition because the magnetic field already induces the second-order parameter component to form a chiral pairing state. We can interpret this property as evidence of the realization of a chiral superconducting phase in SRO. Note that the phase diagram we derived here would be qualitatively identical for the $(p_x + ip_y)$-wave and $(d_{xz} + id_{yz})$-wave states of the forms $\boldsymbol{d}(\boldsymbol{k}) = \Delta_0\hat{\boldsymbol{z}}(k_t \pm ik_p)$ and $\psi(\boldsymbol{k}) = \Delta_0 k_z(k_t \pm ik_p)$, respectively. Despite the nodal structure of the chiral d-wave state, the zero-bias anomaly would appear only in the presence of the perpendicular component like for the chiral p-wave state. Therefore, we consider that the phase diagram in Fig. 1 provides crucial evidence for a chiral superconducting phase in SRO but would not allow us to distinguish decisively between the even- and odd-parity pairing channels.

Based on our discussion we suggest that it would be highly interesting to perform in-plane tunneling experiments for uniaxially strained samples too, in the hope of detecting, by the appearance of a zero-bias peak, the presence of a second transition concurrent with the onset of the μSR signal [47]. Naturally, this observation would depend on which of the two order parameter components nucleates first when the degeneracy is lifted. Therefore, besides the phenomenology in a magnetic field, a comparison of the behaviors of tensile and compressive uniaxial stresses would also provide a test of consistency.

ACKNOWLEDGMENTS

We are grateful to C. W. Hicks, H. Yaguchi, M. Kawamura, V. Grinenko, H.-H. Klauss, K. Ishida, A. P. Mackenzie, S. Kittaka, W. Higemoto, S. Kashiwaya, R. Ishiguro, and Y. Maeno for helpful discussions on their experimental results. We also thank J. Goryo and D. F. Agterberg for their valuable discussions on theoretical aspects. H.K. thanks T. Sakamoto for assistance with the theoretical study. The computational part of this work was performed on the supercomputer SX-ACE at the Cybermedia Center (CMC), Osaka University, which was supported by the Exploratory Research Project for Young Scientists and Female Scientists, CMC, Osaka University. We are also grateful for the financial support from the Core to Core program "Oxide Superspin (OSS)" through the Japan Society for the Promotion of Science (JSPS) and the

Engineering, Physical Sciences Research Council (EPSRC), CCES-IBS, and CNR-SPIN, as well as from a research grant from the Swiss National Science Foundation (SNSF) through Division II (Grants No. 163186 and No. 184739).

[1] Y. Maeno, H. Hashimoto, K. Yoshida, S. Nishizaki, T. Fujita, J. G. Bednorz, and F. Lichtenberg, Nature (London) **372**, 532 (1994).
[2] Y. Maeno, M. Rice, and M. Sigrist, Phys. Today **54**(1), 42 (2001).
[3] A. P. Mackenzie and Y. Maeno, Rev. Mod. Phys. **75**, 657 (2003).
[4] A. P. Mackenzie, T. Scaffidi, C. W. Hicks, and Y. Maeno, npj Quantum Mater. **2**, 40 (2017).
[5] Y. Liu and Z. Q. Mao, Phys. C (Amsterdam, Neth.) **514**, 339 (2015).
[6] G. M. Luke, Y. Fudamoto, K. M. Kojima, M. I. Larkin, J. Merrin, B. Nachumi, Y. J. Uemura, Y. Maeno, Z. Q. Mao, Y. Mori, H. Nakamura, and M. Sigrist, Nature (London) **394**, 558 (1998).
[7] W. Higemoto, A. Koda, R. Kadono, Y. Yoshida, and Y. Ōnuki, JPS Conf. Proc. **2**, 010202 (2014).
[8] J. Xia, Y. Maeno, P. T. Beyersdorf, M. M. Fejer, and A. Kapitulnik, Phys. Rev. Lett. **97**, 167002 (2006).
[9] H. Matsui, M. Yamaguchi, Y. Yoshida, A. Mukai, R. Settai, Y. Onuki, H. Takei, and N. Toyota, J. Phys. Soc. Jpn. **67**, 3687 (1998).
[10] C. Lupien, Ph.D. thesis, University of Toronto, 2002.
[11] B. J. Ramshaw (private communication).
[12] M. Sigrist, Prog. Theor. Phys. **107**, 917 (2002).
[13] M. B. Walker and P. Contreras, Phys. Rev. B **66**, 214508 (2002).
[14] P. G. Kealey, T. M. Riseman, E. M. Forgan, L. M. Galvin, A. P. Mackenzie, S. L. Lee, D. McK. Paul, R. Cubitt, D. F. Agterberg, R. Heeb, Z. Q. Mao, and Y. Maeno, Phys. Rev. Lett. **84**, 6094 (2000).
[15] M. Sigrist and K. Ueda, Rev. Mod. Phys. **63**, 239 (1991).
[16] Here we neglect alternative classification schemes which were put forward recently, taking multiorbital physics into account: A. Ramires and M. Sigrist, Phys. Rev. B **100**, 104501 (2019); W. Huang, Y. Zhou, and H. Yao, *ibid.* **100**, 134506 (2019); S.-O. Kaba and D. Sénéchal, arXiv:1905.10467.
[17] K. Ishida, H. Mukuda, Y. Kitaoka, K. Asayama, Z. Q. Mao, Y. Mori, and Y. Maeno, Nature (London) **396**, 658 (1998).
[18] J. A. Duffy, S. M. Hayden, Y. Maeno, Z. Mao, J. Kulda, and G. J. McIntyre, Phys. Rev. Lett. **85**, 5412 (2000).
[19] A. Pustogow, Y. Luo, A. Chronister, Y.-S. Su, D. A. Sokolov, F. Jerzembeck, A. P. Mackenzie, C. W. Hicks, N. Kikugawa, S. Raghu, E. D. Bauer, and S. E. Brown, Nature **574**, 72 (2019).
[20] K. Ishida, M. Manago, and Y. Maeno, arXiv:1907.12236.
[21] Y. Maeno, S. Kittaka, T. Nomura, S. Yonezawa, and K. Ishida, J. Phys. Soc. Jpn. **81**, 011009 (2012).
[22] S. Kittaka, A. Kasahara, T. Sakakibara, D. Shibata, S. Yonezawa, Y. Maeno, K. Tenya, and K. Machida, Phys. Rev. B **90**, 220502(R) (2014).
[23] K. Machida and M. Ichioka, Phys. Rev. B **77**, 184515 (2008).
[24] K. D. Nelson, Z. Q. Mao, Y. Maeno, and Y. Liu, Science **306**, 1151 (2004).
[25] Y. Liu, New J. Phys. **12**, 075001 (2010).
[26] V. B. Geshkenbein, A. I. Larkin, and A. Barone, Phys. Rev. B **36**, 235 (1987).
[27] J. Jang, D. G. Ferguson, V. Vakaryuk, R. Budakian, S. B. Chung, P. M. Goldbart, and Y. Maeno, Science **331**, 186 (2011).
[28] X. Cai, Y. A. Ying, N. E. Staley, Y. Xin, D. Fobes, T. J. Liu, Z. Q. Mao, and Y. Liu, Phys. Rev. B **87**, 081104(R) (2013).
[29] Y. Yasui, K. Lahabi, M. S. Anwar, Y. Nakamura, S. Yonezawa, T. Terashima, J. Aarts, and Y. Maeno, Phys. Rev. B **96**, 180507(R) (2017)
[30] V. Vakaryuk and A. J. Leggett, Phys. Rev. Lett. **103**, 057003 (2009).
[31] K. Roberts, R. Budakian, and M. Stone, Phys. Rev. B **88**, 094503 (2013).
[32] E. Hassinger, P. Bourgeois-Hope, H. Taniguchi, S. Renè de Cotret, G. Grissonnanche, M. S. Anwar, Y. Maeno, N. Doiron-Leyraud, and L. Taillefer, Phys. Rev. X **7**, 011032 (2017).
[33] K. Deguchi, M. A. Tanatar, Z. Mao, T. Ishiguro, and Y. Maeno, J. Phys. Soc. Jpn. **71**, 2839 (2002).
[34] S. Kittaka, S. Nakamura, T. Sakakibara, N. Kikugawa, T. Terashima, S. Uji, D. A. Sokolov, A. P. Mackenzie, K. Irie, Y. Tsutsumi, K. Suzuki, and K. Machida, J. Phys. Soc. Jpn. **87**, 093703 (2018).
[35] M. Matsumoto and M. Sigrist, J. Phys. Soc. Jpn. **68**, 994 (1999).
[36] A. Furusaki, M. Matsumoto, and M. Sigrist, Phys. Rev. B **64**, 054514 (2001).
[37] C. Kallin and A. J. Berlinsky, J. Phys.: Condens. Matter **21**, 164210 (2009).
[38] C. W. Hicks, J. R. Kirtley, T. M. Lippman, N. C. Koshnick, M. E. Huber, Y. Maeno, W. M. Yuhasz, M. B. Maple, and K. A. Moler, Phys. Rev. B **81**, 214501 (2010).
[39] P. J. Curran, S. J. Bending, W. M. Desoky, A. S. Gibbs, S. L. Lee, and A. P. Mackenzie, Phys. Rev. B **89**, 144504 (2014).
[40] S. Kashiwaya, K. Saitoh, H. Kashiwaya, M. Koyanagi, M. Sato, K. Yada, Y. Tanaka, and Y. Maeno, Phys. Rev. B **100**, 094530 (2019).
[41] S. Lederer, W. Huang, E. Taylor, S. Raghu, and C. Kallin, Phys. Rev. B **90**, 134521 (2014).
[42] W. Huang, S. Lederer, E. Taylor, and C. Kallin, Phys. Rev. B **91**, 094507 (2015).
[43] S. B. Etter, A. Bouhon, and M. Sigrist, Phys. Rev. B **97**, 064510 (2018).
[44] C. W. Hicks, D. O. Brodsky, E. A. Yelland, A. S. Gibbs, J. A. N. Bruin, M. E. Barber, S. D. Edkins, K. Nishimura, S. Yonezawa, Y. Maeno, and A. P. Mackenzie, Science **344**, 283 (2014).
[45] A. Steppke, L. S. Zhao, M. E. Barber, T. Scaffidi, F. Jerzembeck, H. Rosner, A. S Gibbs, Y. Maeno, S. H. Simon, A. P. Mackenzie, and C. W. Hicks, Science **355**, eaaf9398 (2017).
[46] Y.-S. Li, N. Kikugawa, D. A. Sokolov, F. Jerzembeck, A. S. Gibbs, Y. Maeno, C. W. Hicks, M. Nicklas, and A. P. Mackenzie, arXiv:1906.07597.
[47] V. Grinenko, S. Ghosh, R. Sarkar, J.-C. Orain, A. Nikitin, F. Brückner, J. Park, M. Barber, N. Kikugawa, D. Sokolov, J. S. Bobowski, T. Miyoshi, Y. Maeno, A. P. Mackenzie, H. Luetkens, C. W. Hicks, and H.-H. Klauss (unpublished).

[48] Y. Maeno, T. Ando, Y. Mori, E. Ohmichi, S. Ikeda, S. NishiZaki, and S. Nakatsuji, Phys. Rev. Lett. **81**, 3765 (1998).
[49] H. Yaguchi, M. Wada, T. Akima, Y. Maeno, and T. Ishiguro, Phys. Rev. B **67**, 214519 (2003).
[50] H. Yaguchi, K. Takizawa, M. Kawamura, N. Kikugawa, Y. Maeno, T. Meno, T. Akazaki, K. Semba, and H. Takayanagi, J. Phys. Soc. Jpn. **75**, 125001 (2006).
[51] M. Sigrist and H. Monien, J. Phys. Soc. Jpn. **70**, 2409 (2001).
[52] S. S. Ghosh, Y. Xin, Z. Q. Mao, and E. Manousakis, Phys. Rev. B **96**, 184506 (2017).
[53] Y. A. Ying, N. E. Staley, Y. Xin, K. Sun, X. Cai, D. Fobes, T. J. Liu, Z. Q. Mao, and Y. Liu, Nat. Commun. **4**, 2596 (2013).
[54] Z. Q. Mao, K. D. Nelson, R. Jin, Y. Liu, and Y. Maeno, Phys. Rev. Lett. **87**, 037003 (2001).
[55] M. Kawamura, H. Yaguchi, N. Kikugawa, Y. Maeno, and H. Takayanagi, J. Phys. Soc. Jpn. **74**, 531 (2005).
[56] J. Hooper, Z. Q. Mao, K. D. Nelson, Y. Liu, M. Wada, and Y. Maeno, Phys. Rev. B **70**, 014510 (2004).
[57] H. Kaneyasu, N. Hayashi, B. Gut, K. Makoshi, and M. Sigrist, J. Phys. Soc. Jpn. **79**, 104705 (2010).
[58] H. Kaneyasu, S. B. Etter, T. Sakai, and M. Sigrist, Phys. Rev. B **92**, 134515 (2015).
[59] H. Yaguchi, K. Takizawa, M. Kawamura,, N. Kikugawa, Y. Maeno, T. Meno, T. Akazaki, K. Semba, and H. Takayanagi, in *24th International Conference on Low Temperature Physics - LT24*, edited by Y. Takano, S. P. Hershfield, S. O. Hill, P. J. Hirschfeld, and A. M. Goldman, AIP Conf. Proc. No. 850 (AIP, New York, 2006), p. 543.
[60] M. Matsumoto, C. Belardinelli, and M. Sigrist, J. Phys. Soc. Jpn. **72**, 1623 (2003).
[61] Y. Tanaka and S. Kashiwaya, Rep. Prog. Phys. **63**, 1641 (2000).
[62] M. Sigrist, Prog. Theor. Phys. Suppl. **160**, 1 (2005).
[63] Y. A. Ying, Y. Xin, B. W. Clouser, E. Hao, N. E. Staley, R. J. Myers, L. F. Allard, D. Fobes, T. Liu, Z. Q. Mao, and Y. Liu, Phys. Rev. Lett. **103**, 247004 (2009).
[64] H. Kaneyasu, Y. Enokida, T. Nomura, Y. Hasegawa, T. Sakai, and M. Sigrist, Proceedings for International Conference on Strongly Correlated Electron Systems 2019 - SCES'19 (unpublished).